Electronic Supplementary Material (ESI) for Analytical Methods.

Supporting Information

Visualized sensor based on layered double hydroxides with peroxidase-like activity for sensitive acetylcholinesterase assay

Hao Cheng[a,b], Yuying Wang[a,b], Yue Wang[a], Lei Ge[a], Xiaojuan Liu*[a] and Feng Li *[a]

[a.]College of Chemistry and Pharmaceutical Sciences, Qingdao Agricultural University, Qingdao 266109, P. R. China.

[b.]College of plant health & medicine, Qingdao Agricultural University, Qingdao 266109, P. R. China.

* Corresponding author. Tel/Fax: 86-532-58957855

E-mail: xjliu@qau.edu.cn (Xiaojuan Liu); lifeng@qau.edu.cn (Feng Li);

Contents

Experimental section

Chemicals and materials

Cobalt chloride hexahydrate ($CoCl_2 \cdot 6H_2O$), nickel chloride hexahydrate ($NiCl_2 \cdot 6H_2O$), ammonia solution ($NH_3 \cdot 6H_2O$), Hepes ($C_8H_{18}N_2O_4S$), o-Phenylenediamine (OPD), 3,3',5,5'-Tetramethylbenzidine (TMB), 2,2'-Azinobis-(3-ethylbenzthiazoline-6-sulphonate) (ABTS), H_2O_2 (30%), and NaOH with analytical grade were obtained from Sinopharm Chemical Reagent Co., Ltd. (Shanghai, China). Bovine serum albumin (BSA), glucose oxidase (GOX), lambda exonuclease (λ-Exo), thrombin, nicking endonuclease (Nt.BbvCI) were purchased form New England Biolabs Inc. (Beijing, China). Acetylcholinesterase (AChE) from electric eel were obtained from Aladdin Industrial Corporation (Shanghai, China). Ultrapure water (resistivity ≥18.2 MΩ·cm at 25 °C) used in the experiments was obtained from a Milli-Q water purification system (Millipore Corp., Bedford, MA, USA).

Instruments

All the UV-vis spectra were gotten from an UV-1800 spectrophotometer (Shimadzu, Japan). Scanning electron microscopy (SEM) images and energy dispersive spectroscopy (EDS) were performed on a JSM-IT500 field-emission scanning electron microscopy equipped with an EDS detector (Hitachi, Japan). Transmission electron microscopy (TEM) was measured using the HT7700 microscope (Hitachi, Japan). X-ray diffraction (XRD) patterns were taken on a Bruker D8 Advance X-ray diffractometer (Bruker, Germany). Zeta potential was tested on a Zetasizer Nano ZEN3690 (Malvern Instruments Ltd., Malvern, UK), in which the pH of the Ni/Co LDHs (0.2 mg mL^{-1}, 1 mL) and the mixture of Ni/Co LDHs (0.2 mg mL^{-1}, 1 mL)/AChE (0.2 mg mL^{-1}, 1 mL) were adjusted to 7, 8, 9, and 10 by adding NaOH, respectively. X-ray photoelectron

spectroscopy (XPS) spectra were recorded on Thermo Scientific ESCALAB Xi+ spectrometer.

Peroxidase-like activity of Ni/Co LDHs

The peroxidase-like activity of Ni/Co LDHs was measured by monitoring the absorbance of oxOPD at 420 nm as detailed below. First, Ni/Co LDHs (100 μL, 1.0 mg mL^{-1}), H_2O_2 (100 μL, 5 mM), and Hepes (200 μL, 10 mM, pH = 9.0) was added to 2 mL centrifuge tube, followed by the addition of OPD (100 μL, 5 mM). The resulted solution was allowed to react at 37 ℃ for 10 min in the dark. Finally, the absorbance of the solution at 420 nm was detected by UV-1800 spectrophotometer. Similarly, the peroxidase-like activity of Ni/Co LDHs was also measured by using TMB and ABTS as the chromogenic agents with similar procedures like OPD.

Kinetic study of Ni/Co LDHs nanozyme

Using H_2O_2 and OPD as the substrates, the kinetics was investigated by monitoring the absorbance of the system at 420 nm. When OPD was used as the substrate, OPD with different concentrations were added into the Hepes buffer solution with 1 mg mL^{-1} Ni/Co LDHs and 5 mM H_2O_2. Similarly, when H_2O_2 was used as the substrate, the concentration of OPD was fixed to be 5 mM. Then, the absorbance at 420 nm was recorded after incubating at 37 ℃ for 10 min. The Michaelis–Menten constant was calculated using a Lineweaver–Burk plot:

$$1/\nu = K_m/V_{max}(1/[S] + 1/K_m)$$

where ν is the initial velocity, V_{max} represents the maximal reaction velocity, [S] is the substrate concentration, K_m is Michaelis–Menten constant, which is an indicator of enzyme affinity for its substrate. The smaller the value of K_m, the stronger the affinity between the enzyme and the substrate.

Fetal bovine serum sample assay

For fetal bovine serum samples detection, aliquots of AChE stock solution were dissolved in 10% bovine serum according to the standard addition method. The final concentrations of AChE were 0, 220, 1100, and 4400 μU mL^{-1} in the spiked serum samples. The absorbance of the proposed sensor towards these serum samples were recorded and the recoveries were calculated.

Supporting tables

Table S1. Comparison of K_m of different nanozymes.

Catalyst	K_m (mM)		References
	OPD	H_2O_2	
HRP	0.59	0.34	S1
MnO_2	0.31	0.12	S1
Ag/Pt NPs	0.129	76.05	S2
$Au_1Ag_4Pd_1$	10.61	0.52	S3
GOx−Fe_3O_4@SHS	12.1	-	S4
Cu-CDs	0.588	-	S5
Ni/Co LDHs	0.213	0.327	This work

Table S2. Comparison of the analytical performance for the detection of AChE by the as-proposed method and those reported in literature.

Strategy	Method	Linear range (μU mL^{-1})	LOD (μU mL^{-1})	Ref.
ICT-ESIPT-based fluorescence sensor	Fluorescence	---	2×10^5	S6
Fluorescence assay based on glutathione-capped gold nanoclusters	Fluorescence	30-3×10^4	30	S7
A ratiometric fluorescence probe based on graphene quantum dots and o-phenylenediamine	Fluorescence	2000-4500	90	S8
Ag^+@CTAB-AuNPs system-based colorimetric detection	Colorimetric	75-2.5×10^4	75	S9
Au-decorated N-rich carbon dots as peroxidase mimics	Colorimetric	100-5000	107	S10
Acetylcholine-based colorimetric detection	Colorimetric	2000-1.4×10^4	500	S11
Cobalt oxyhydroxide nanoflakes-based sensitive colorimetric sensor	Colorimetric	100-5000	33	S12
A pendant droplet-based sensor	Pendant droplet	100-1×10^6	170	S13
Photoelectrochemical sensor based on CdS quantum dots	Photoelectrochemical	10-1000	10	S14
Highly selective SERS detection based on catalytic reaction	SERS	2×10^4-4.8×10^6	2×10^4	S15
Colorimetric sensor based on peroxidase-mimicking Ni/Co LDHs nanozyme	Colorimetric	22-2.2×10^5	6.6	This work

Table S3. Recovery data for blank extraction samples of fetal bovine serum (without add AChE) spiked with different concentrations of AChE (n=5).

Sample number	AChE added ($\mu U\ mL^{-1}$)	AChE detected ($\mu U\ mL^{-1}$)	Recovery (%)	RSD
1	0	0	---	---
2	220	230	105	2.9
3	1100	1190	108	3.0
4	4400	4360	99	1.5

Supporting figures

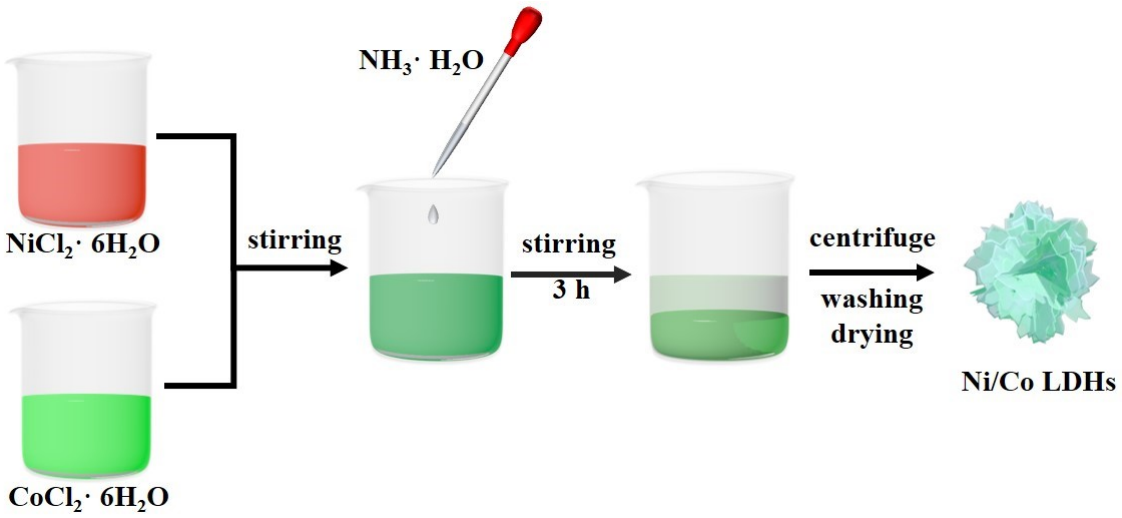

Fig. S1. Synthesis schematic of the preparation process of Ni/Co LDHs.

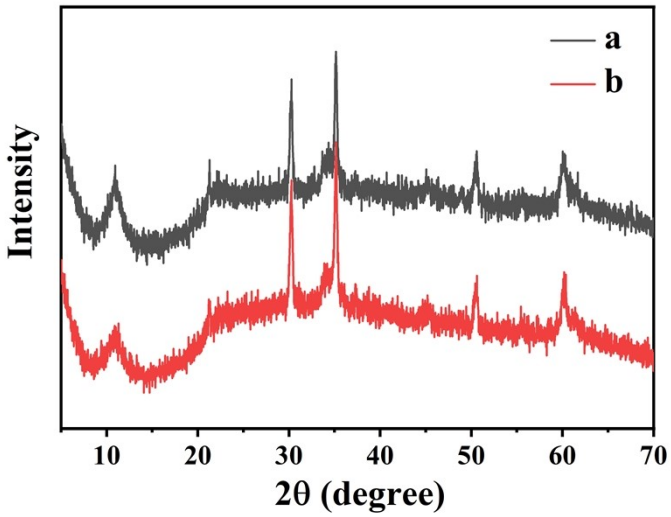

Fig. S2. XRD patterns of Ni/Co LDHs before (a) and after (b) adding AChE.

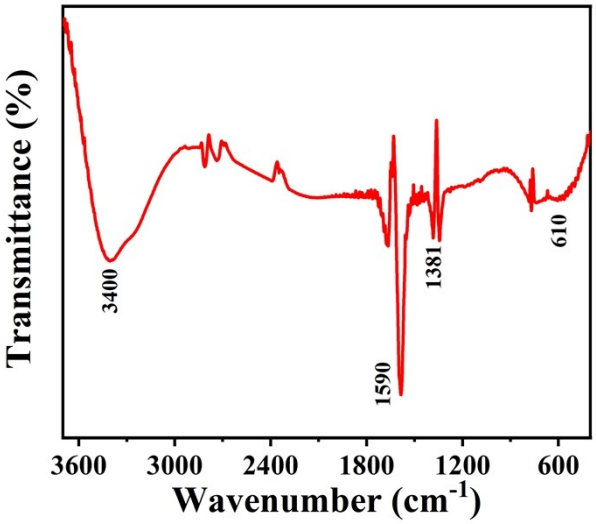

Fig. S3. FTIR spectrum of Ni/Co LDHs.

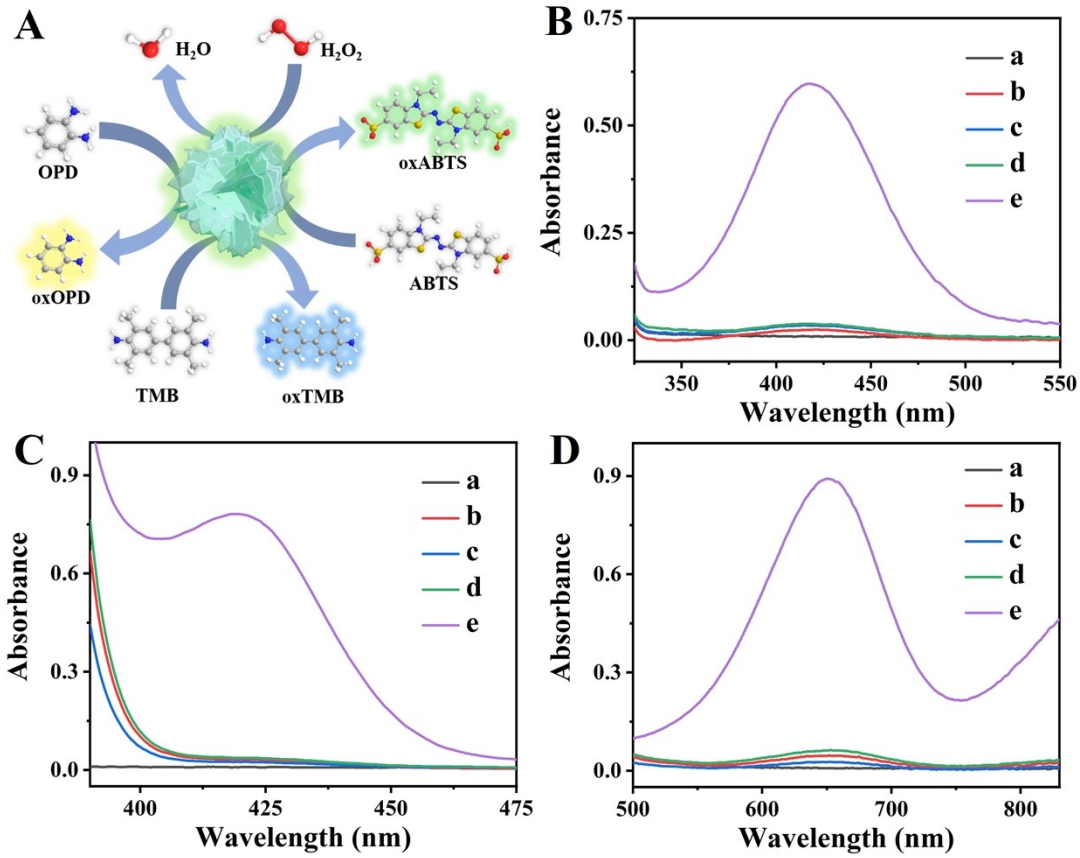

Fig. S4. Study on the peroxidase-like catalytic ability of Ni/Co LDHs. (A) The schematic illustration of the peroxidase-like actibity; (B) the UV-vis absorption spectra of (a) Ni/Co LDHs only, (b) OPD only, (c) LDHs and OPD solution under N_2 atmosphere, (d) LDHs and OPD solution under O_2 atmosphere, (e) LDHs, OPD, and H_2O_2 solution under N_2 atmosphere; (C) the UV-vis absorption spectra of (a) Ni/Co LDHs only, (b) ABTS only, (c) LDHs and ABTS solution under N_2 atmosphere, (d) LDHs and ABTS solution under O_2 atmosphere, (e) LDHs, ABTS, and H_2O_2 solution under N_2 atmosphere; (D) the UV-vis absorption spectra of (a) Ni/Co LDHs only, (b) TMB only, (c) LDHs and TMB solution under N_2 atmosphere, (d) LDHs and TMB solution under O_2 atmosphere, (e) LDHs, TMB, and H_2O_2 solution under N_2 atmosphere.

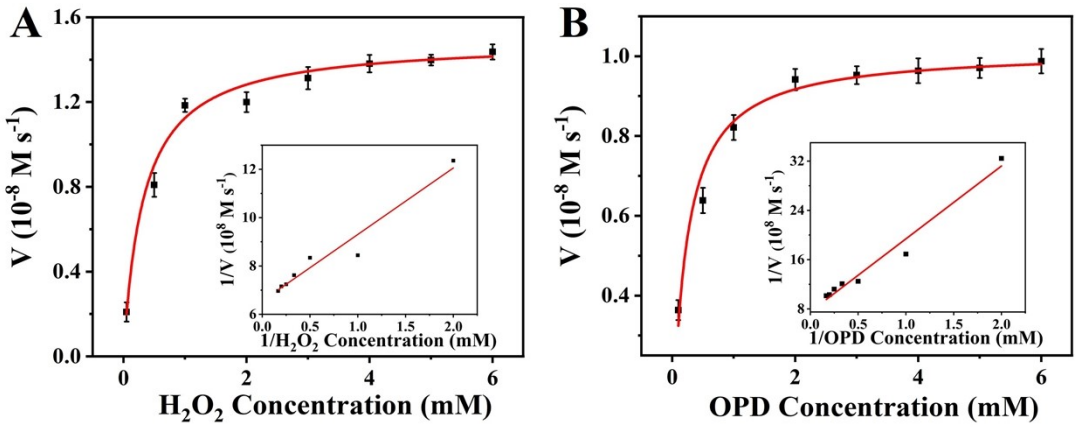

Fig. S5. The steady-state kinetics analysis. (A, B) Michaelis–Menten curves from activity data of (A) the fixed concentration of OPD (5 mM) and various concentrations of H_2O_2 (0.05–6 mM); (B) the fixed concentration of H_2O_2 (5 mM) and various concentrations of OPD (0.1–6 mM); The inset shows the corresponding double-reciprocal plots for the calculation of enzyme kinetic parameters by the Michaelis–Menten equation. The error bars represent the standard deviation of three measurements.

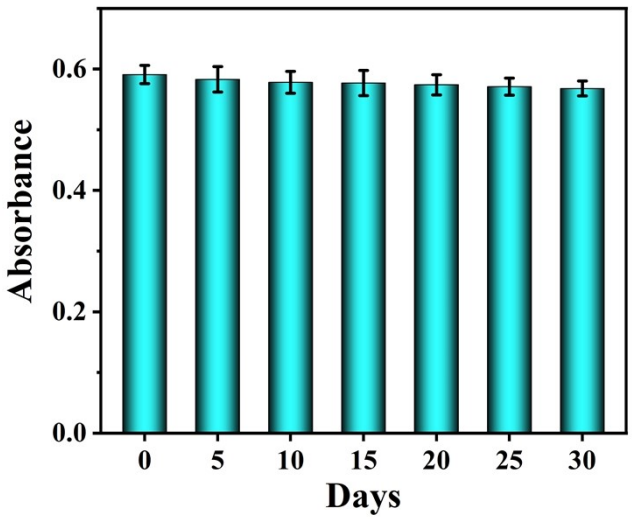

Fig. S6. Absorbance of the OPD solution at 420 nm after catalyzed by the Ni/Co LDHs stored at -4 ℃for different days: 0, 5, 10, 15, 20, 25, and 30 days, respectively.

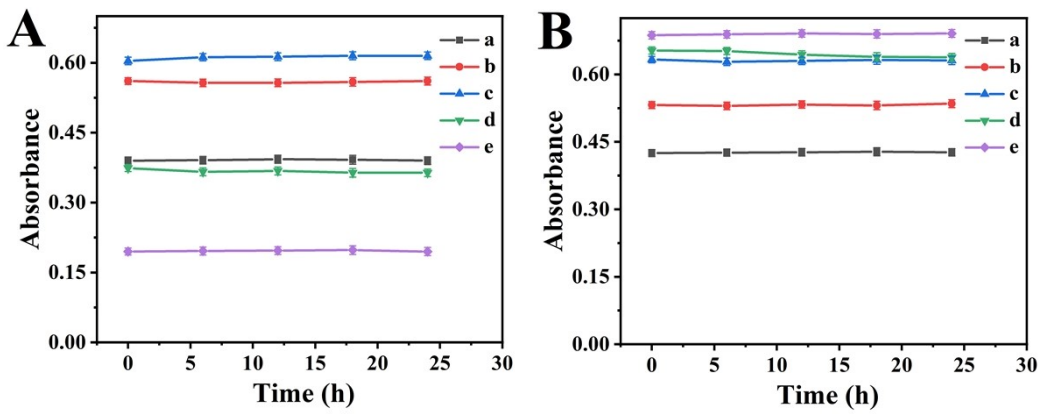

Fig. S7. Absorbance of the OPD solution at 420 nm after catalyzed by the Ni/Co LDHs stored in (A) different pH buffer for different hours: (a) 7, (b) 8, (c) 9, (d) 10, and (e) 11; (B) different temperature for different hours: (a) 20, (b) 25, (c) 30, (d) 35, and (e) 40 ℃.

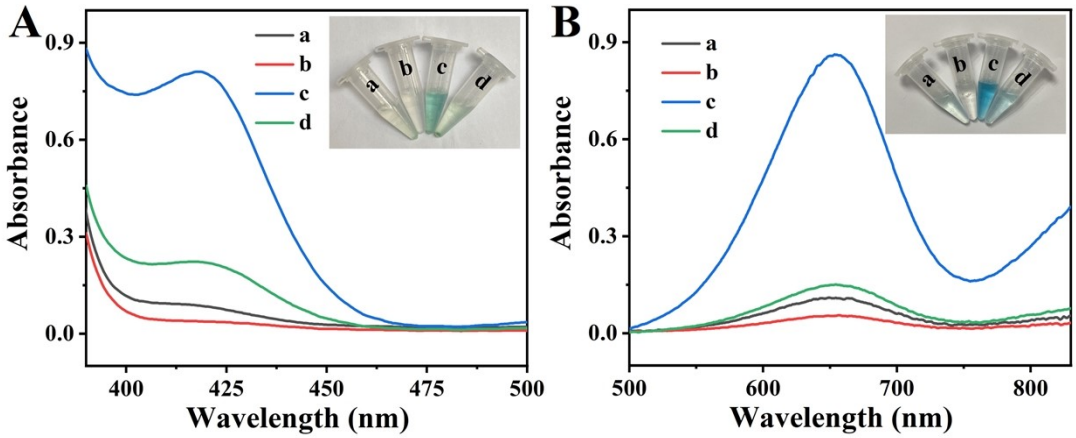

Fig. S8. Absorbace of the sensing system under different conditions in the presence of: (A) (a) LDHs and ABTS, (b) H_2O_2 and ABTS, (c) LDHs, H_2O_2 and ABTS, (d) LDHs, H_2O_2, ABTS, and AChE, respectively; (B) (a) LDHs and TMB, (b) H_2O_2 andTMB, (c) LDHs, H_2O_2 and TMB, (d) LDHs, H_2O_2, TMB, and AChE, respectively.

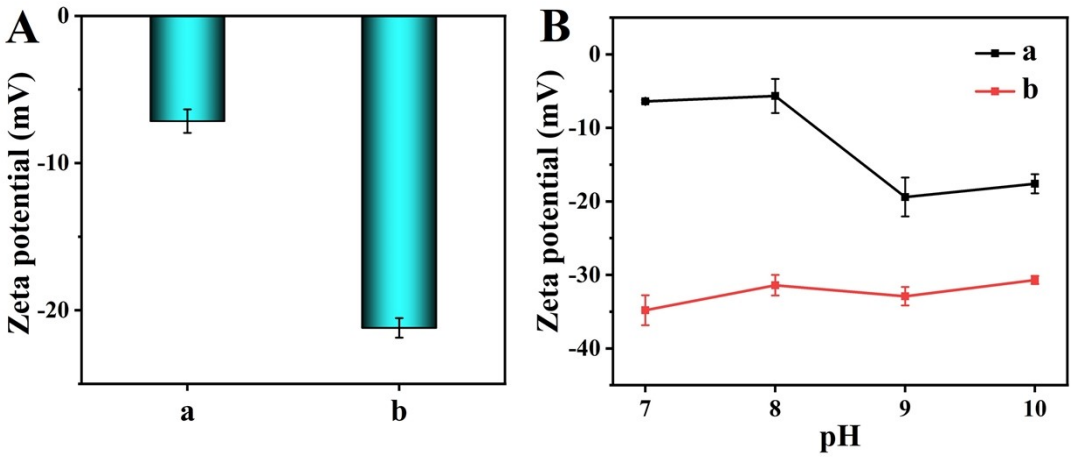

Fig. S9. (A) Zeta potential value of LDHs (a) and LDHs/AChE (b); (B) zeta potential of LDHs (a) and LDHs/AChE (b) under different pH.

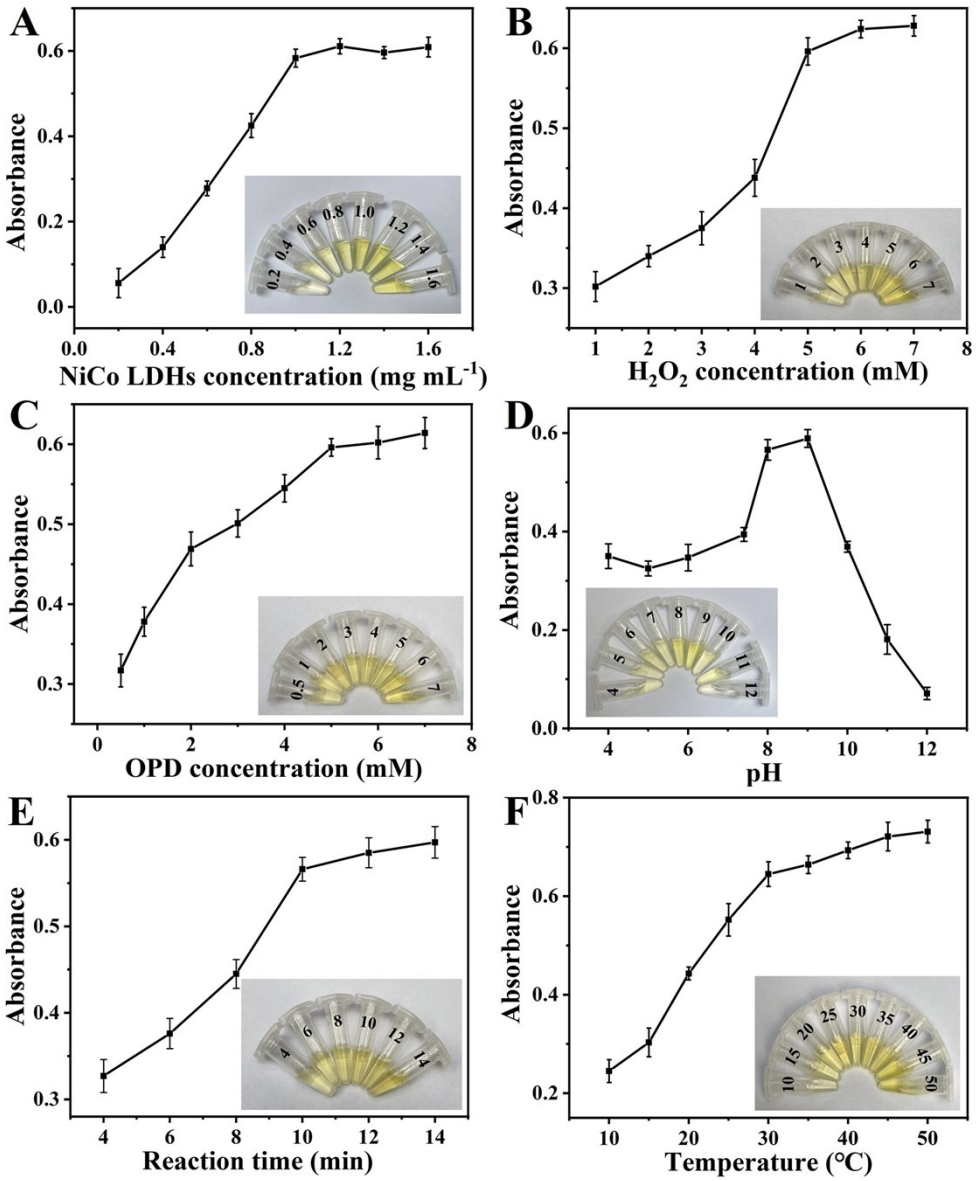

Fig. S10. Absorbance variation obtained under different conditions: (A) Ni/Co LDHs concentrations:0.2, 0.4, 0.8, 1.0, 1.2, 1.4, and 1.6 mg mL^{-1}; (B) H_2O_2 concentrations: 1, 2, 3, 4, 5, 6, and 7 mM; (C) OPD concentrations:0.2, 0.4, 0.8, 1.0, 1.2, 1.4, and 1.6 mg mL^{-1}; (D) pH: 4, 5, 6, 7.4, 8, 9, 10, 11, and 12; (E) reaction time: 4, 6, 8, 10, 12, and 14 min; (F) temperature: 10, 15, 20, 25, 30, 35, 40, 45, and 50 ℃.

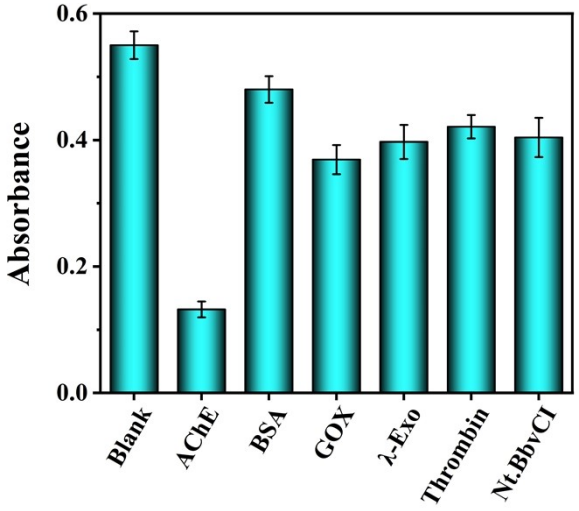

Fig. S11. The influence of catalytical performance in the absence (blank) and presence of different protein: AChE, BSA, GOX, λ-Exo, thrombin, Nt.BbvCI with the same concentration.

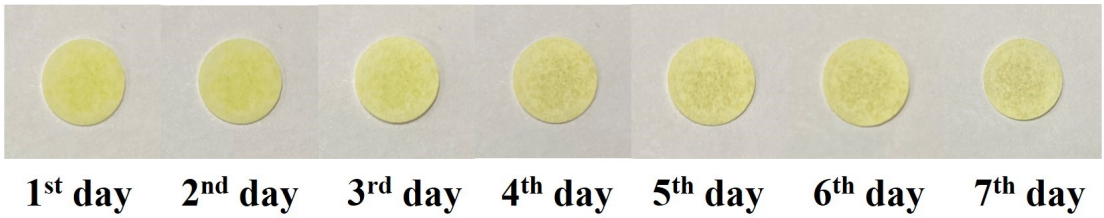

Fig. S12. The color response of the paper-based biosensor after storing at room temperature for seven days.

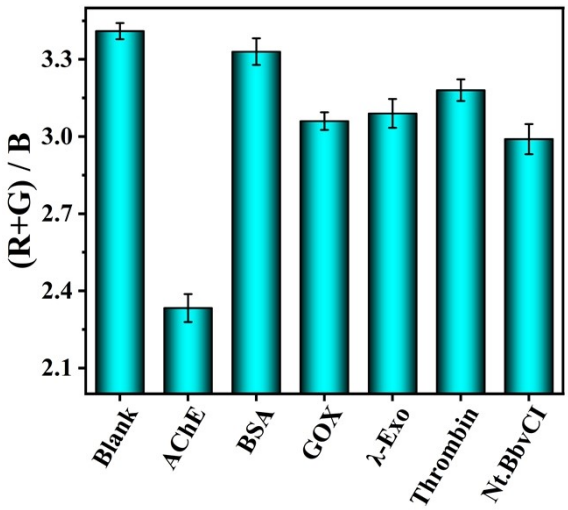

Fig. S13. The (R+G)/B value in the absence (blank) and presence of different protein: AChE, BSA, GOX, λ-Exo, thrombin, Nt.BbvCI with the same concentration.

References

S1. X. Liu, Q. Wang, H. H. Zhao, L. C. Zhang, Y. Y. Su, Y. Lv, BSA-templated MnO_2 nanoparticles as both peroxidase and oxidase mimics, *Analyst*, 2012, **137**, 4552−4558.

S2. M. Gharib, A. Kornowski, H. Noei, W. J. Parak, I. Chakraborty, Protein-protected porous bimetallic AgPt nanoparticles with pH-switchable peroxidase/catalase-mimicking activity, *ACS Materials Lett*., 2019, **1**, 310−319.

S3. J. Kong, J. Zheng, Z. M. Li, J. B. Huang, F. H. Cao, Q. Zeng, F. Li, One-pot synthesis of AuAgPd trimetallic nanoparticles with peroxidase-like activity for colorimetric assays, *Anal. Bioanal. Chem*., 202, **1413**, 5383−5393.

S4. G. Begum, P. Swathi, A. K. Bandarapu, J. Nayak, R. K. Rana, Spatial confinement of enzyme and nanozyme in silica-based hollow microreactors, *ACS Appl. Mater. Interfaces*, 2020, **12**, 45476−45484.

S5. D. Z. Yang, Q. L. Li, S. K. Tammina, Z. Gao, Y. L. Yang, Cu-CDs/H_2O_2 system with peroxidase-like activities at neutral pH for the cocatalytic oxidation of O-phenylenediamine and inhibition of catalytic activity by Cr(III), *Sens. Actuators B Chem*., 2020, **319**, 128273.

S6. W. Q. Meng, Z. P. Pei, Y. R. Wang, M. X. Sun, Q. Q. Xu, J. F. Cen, K. Guo, K. Xiao, Z. J. Li, Two birds with one stone: The detection of nerve agents and AChE activity with an ICT-ESIPT-based fluorescence sensor, *J. Hazard. Mater*., 2021, **410**, 124811.

S7. R. L. Zhang, S. S. Liang, M. Jin, T. He, Z. Q. Zhang, Simple and sensitive fluorescence assay for acetylcholinesterase activity detection and inhibitor screening based on glutathione-capped gold nanoclusters, *Sens. Actuators B Chem*., 2017, **253**, 196−202.

S8. M. S. Ye, B. X. Lin, Y. Yu, H. Li, Y. M. Wang, L. Zhang, Y. J. Cao, M. L. Guo, A ratiometric fluorescence probe based on graphene quantum dots and o-phenylenediamine for highly sensitive detection of acetylcholinesterase activity, *Microchim. Acta*, 2020, **187**, 511.

S9. J. J. Zhang, W. S. Zheng, X. Y. Jiang, Ag^{+}-gated surface chemistry of gold nanoparticles and colorimetric detection of acetylcholinesterase, *Small*, 2018, **14**, 1801680.

S10. D. D. Zhang, Q. Y. Han, W. D. Liu, K. Y. Xu, M. Z. Shao, Y. Y. Li, P. Y. Du, Z. Zhang, B. S. Liu, L. B. Zhang, X. Q. Lu, Au-decorated N-rich carbon dots as peroxidase mimics for the detection of acetylcholinesterase activity, *ACS Appl. Nano Mater*., 2022, **5**, 1958−1965.

S11. T. Han, G. F. Wang, Peroxidase-like activity of acetylcholine-based colorimetric detection of acetylcholinesterase activity and an organophosphorus inhibitor, *J. Mater. Chem. B*, 2019, **7**, 2613−2618.

S12. R. Jin, Z. H. Xing, D. S. Kong, X. Yan, F. M. Liu, Y. Gao, P. Sun, X. S. Liang, G. Y. Lu, Sensitive colorimetric sensor for point-of-care detection of acetylcholinesterase using cobalt oxyhydroxide nanoflakes, *J. Mater. Chem. B*, 2019, **7**, 1230−1237.

S13. B. Y. Li, Y. X. Guo, Y. F. Jiang, J. M. Lin, Q. Z. Hu, L. Yu, A pendant proplet-based sensor for the detection of acetylcholinesterase and its inhibitors, *Chem. Commun*., 2021, **57**, 8909−8912.

S14. T. Hou, L. F. Zhang, X. Z. Sun, F. Li, Biphasic photoelectrochemical sensing strategy based on in situ formation of CdS quantum dots for highly sensitive detection of acetylcholinesterase activity and inhibition, *Biosens. Bioelectron*., 2016, **75**, 359−364.

S15. Y. Chen, W. F. Zhao, J. C. Si, Y. N. Zheng, H. Tan, F. N. Meng, G. H. Yang, Y. Q. Gu, L. L. Qu, Highly selective SERS detection of acetylcholinesterase in human blood based on catalytic reaction, *Anal. Chim. Acta*, 2022, **1232**, 340495.